Article

Adjustment and Assessment of the Measurements of Low and High Sampling Frequencies of GPS Real-Time Monitoring of Structural Movement

Mosbeh R. Kaloop [1,2,3], Jong Wan Hu [1,2,]* and Emad Elbeltagi [4,5]

[1] Department of Civil and Environmental Engineering, Incheon National University, 22012 Incheon, Korea; mosbeh.kaloop@gmail.com
[2] Incheon Disaster Prevention Research Center, Incheon National University, 22012 Incheon, Korea
[3] Department of Public Works and Civil Engineering, Mansoura University, 35516 Mansoura, Egypt
[4] Department of Structural Engineering, Mansoura University, 35516 Mansoura, Egypt; eelbelta@mans.edu.eg
[5] Department of Civil Engineering, Mansoura Higher Institute for Engineering and Technology, 35111 Talkha, Egypt
* Correspondence: jongp24@incheon.ac.kr; Tel.: +82-32-835-8463

Abstract: Global Positioning System (GPS) structural health monitoring data collection is one of the important systems in structure movement monitoring. However, GPS measurement error and noise limit the application of such systems. Many attempts have been made to adjust GPS measurements and eliminate their errors. Comparing common nonlinear methods used in the adjustment of GPS positioning for the monitoring of structures is the main objective of this study. Nonlinear Adaptive-Recursive Least Square (RLS), extended Kalman filter (EKF), and wavelet principal component analysis (WPCA) are presented and applied to improve the quality of GPS time series observations. Two real monitoring observation systems for the Mansoura railway and long-span Yonghe bridges are utilized to examine suitable methods used to assess bridge behavior under different load conditions. From the analysis of the results, it is concluded that the wavelet principal component is the best method to smooth low and high GPS sampling frequency observations. The evaluation of the bridges reveals the ability of the GPS systems to detect the behavior and damage of structures in both the time and frequency domains.

Keywords: GPS; RLS; EKF; wavelet; dynamic; structural health monitoring

1. Introduction

Global Positioning System (GPS) is a common geodetic observation method used to assess and evaluate the static, semi-static, and dynamic behaviors of structures under different load cases using real-time observation. The advantages of GPS monitoring systems for the dynamic monitoring of structures can be found in [1,2]. The main advantage of a GPS monitoring system is the measurement of monitoring point coordinates in time series; in addition, the full movements in the time domain can be measured. However, the main disadvantage of using GPS systems is the error and noise associated with their measurements. The performance of GPS monitoring of structures in terms of error and noise is presented in [3–5]. Commercial GPS software systems can eliminate short baseline measurement errors, but measurement noise and remaining errors still contaminate the dynamic measurements of a GPS. This study focuses on eliminating GPS measurement noises after preprocessing by the GPS software.

Studying the behavior of structures in terms of measurement, assessment, maintenance, and serviceability is called structural health monitoring (SHM). GPS-SHM with high sampling frequency

has an enormous advantage compared with conventional instruments for monitoring the deformation, displacement, and vibration of structures. Recently, a 10 to 100 Hz-GPS sampling frequency has been utilized and assessed to monitor the behavior of structures [6–9]. Moschas and Stiros [6] estimated the dynamic behavior of short-span bridges using a 10 Hz-GPS sampling frequency. Yu et al. [7] and Kaloop and Li [9] monitored short-, medium-, and long-span bridges using a 20 Hz GPS sampling frequency. They concluded that the accuracy of the GPS observations can be estimated up to the sub-millimeter level when monitoring the vibration response of short-, medium-, and long-span bridges. Moschas and Stiros [8] utilized the 100 Hz sampling frequency to assess a footbridge and found that the deflection can be measured up to a few millimeters for a natural frequency of the bridge up to 7 Hz. Yi et al. [10] evaluated the 50 and 100 Hz GPS sampling frequencies to assess the performance of static and dynamic behavior and found that the high sampling frequency is applicable to estimate the behavior of stiff and flexible structures. This paper studies the sensitivity of low and high sampling frequency GPS measurements, 1 and 20 Hz, in the time and frequency domains. The results will help to assess suitable GPS monitoring systems for use based on quality, availability, and cost.

To evaluate structures based on GPS monitoring systems, the processing of GPS measurements mainly uses filtering and smoothing to eliminate the effects of GPS error and noise. Kaloop and Hu [11] utilized neural network filters to estimate the dynamic performance of a long-span bridge and found that the neural networks can be used to eliminate the GPS noise. Moschas and Stiros [3,6,8] de-noised the time series of displacement measurements using a moving average and band-pass filter to observe the semi-static and dynamic displacement components of short spans. Yu et al. [7] used a multimode adaptive filter to estimate the behavior of short- and medium-span bridges, and they found that the proposed algorithm can improve the accuracy of the GPS measurements. Feng et al. [12] applied the extended Kalman filter (EKF) to identify different levels of damage to a large-scale bridge caused by earthquake motions. EKF is also reported to be a good tool to eliminate GPS noise and error [12,13]. Wavelet analysis is used to analyze the behavior of structures and evaluate their performance [14,15]. Ogundipe et al. [16] utilized the wavelet method to denoise GPS data collected from a cable stayed bridge. Kaloop and Kim [17] applied wavelet principal component analysis to estimate the behavior of a railway bridge and denoise the GPS measurement error and dynamic noise associated with the structure movements. Moreover, many GPS measurement filtering and smoothing methods are applied to estimate the accurate static and dynamic behavior of structures [13,18,19], and GPS integration with accelerometer measurements is also studied [20–22]. Therefore, in this study, three common de-noise filtering and smoothing methods, non-linear Adaptive-Recursive Least Square, EKF, and wavelet principal component analysis, are compared to identify the most suitable approach for extracting structure behavior components in the time and frequency domains.

The paper is organized as follows: Section 2 summarizes three common methods used to smooth and filter GPS measurements. Section 3 presents the designed experimental study to evaluate the performance of the three methods. The description and the evaluation of the real-time monitoring of two case studies with different loads are also presented in Section 3. Then, the conclusions are presented in Section 4.

2. Methodology

GPS measurements of structure movement are divided into semi-static (long-period), short-period, and dynamic components [23]. Therefore, to calculate the long-period movement component, the measurements should be filtered or smoothed. Three common methods to extract the long-period components are presented and evaluated in the following sub-sections.

2.1. Adaptive-Recursive Least Square Filter

Traditional least squares estimation methods for structural behavior can be used to extract actual response time series and compare the result to the measured signals. The recursive least

square (RLS) filter is one of the least square (LS) algorithms. This method has been proven to be better than other LS algorithms at extracting highly accurate measurements [24]. The RLS is developed and improved using an adaptive recursive algorithm to estimate a weight vector for the filter iteration [24,25]. The second-order Volterra RLS adaptive filter is most popular for identifying the nonlinear performance of structures [26,27]. The exponential error differentiation is used to estimate the filter coefficient in this algorithm, which is dependent on the correlation matrix *P(t)* of the input signal and the cross-correlation matrix of the input *x(t)* and desired *d(t)* signals. In this study, the RLS with second-order Volterra filter is applied to estimate the nonlinear dynamic behavior of structures based on GPS monitoring systems. The GPS time series (*x(t)* (*t* = 1, 2, . . . , n)) adjustment based on RLS focused on the updated weight matrix (*w(t)*) and the gain vector (*k* (*t*)). Table 1 summarizes the nonlinear RLS process [28,29]. To compute the adjusted movements of the structure (*y(t)*) and estimate the measurement errors *e(t)*, the desired response at time *d(t)* is calculated based on input measurements [29]. The desired signals are calculated using the finite impulse response (FIR) filter identification system [7,30]. Furthermore, the initial weight (*w(0)*) and the forgetting factor (λ) values are assumed to be 0 and 1, respectively. The value *δ* is a regularization parameter; a positive constant indicates a high signal-to-noise ratio (SNR) and a negative constant a low SNR. Herein, *δ* is assumed to be a small positive value.

Table 1. Proposed RLS adjustment of GPS time series.

Given *d(t)* and *x(t)*; Choose λ (forgetting factor (0 < ˘ ≤ 1)), *P* (0) = ffi*I*, while I is the *n-by-n* identity matrix; then compute:
$e\left(t\right) = d\left(t\right) - x^T\left(t\right)w\left(t-1\right)$ $k\left(t\right) = \dfrac{\lambda^{-1}P^{-1}(t-1)x(t)}{1+\lambda^{-1}x^T(t)P^{-1}(t-1)x(t)}$ $w\left(t\right) = w\left(t-1\right) + k\left(t\right)e\left(t\right)$ $P^{-1}\left(t\right) = \lambda^{-1}P^{-1}\left(t-1\right) - \lambda^{-1}k\left(t\right)x^T\left(t\right)P^{-1}\left(t-1\right)$ $y\left(t\right) = w^T\left(t\right)x\left(t\right)$

2.2. Extended Kalman Filter

The Kalman filter (KF) is a common filter used to detect the accurate positions of point movements [31]. The EKF is a KF type applied to estimate structure performance, especially their nonlinear behavior. The EKF is the standard Bayesian state-estimation algorithm for nonlinear systems in civil engineering applications [32,33]. The first-order linearization of the state transition and observation matrices of the nonlinear system is a main concept of the EKF [31]. For real-time GPS measurements, the stochastic n-state discrete time system is considered, which embodies the system (Equation (1)) and measurement (Equation (2)) [29] as follows:

$$x_t = f(x_{t-1}) + w_{t-1} \tag{1}$$

$$y_t = h(x_t) + v_t \tag{2}$$

where x_t is the state vector, y_t is the measurement vector at time *t*, $w_{t-1} \sim N(0, Q_{t-1})$ is the Gaussian process noise, $v_t \sim N(0, R_{t-1})$ is the Gaussian measurement noise, *t* = 1, 2, . . . , n, *f*(.) is the dynamic model function, and *h*(.) is the measurement function. The forward filter process is implemented based on the linearized state and measurement vectors with Taylor series expansions [29,32]. In this study, nonlinear dynamic systems are linearized using a Jacobian complex step. The EKF time and measurement update are processed to achieve the optimal estimates of the GPS positioning as shown in Table 2 [31,34].

Table 2. Proposed EKF adjustment of the GPS-time series.

Assume the last filtered state estimation $\hat{x}_{t/t}$.
Linearize the system dynamics, $\hat{x}_{t-1} = f(\hat{x}_t) + w_t$ around $\hat{x}_{t/t}$
Apply the prediction step of the KF to the linearized obtained system dynamics, yielding $\hat{x}_{t+1/t}$ and $P_{t+1/t}$, where P is an error covariance matrix.
Linearize the observation dynamics, $y_t = h(x_t) + v_t$ around $\hat{x}_{t+1/t}$.
Apply KF to the linearized observation dynamics, yielding $\hat{x}_{t+1/t+1}$ and $P_{t+1/t+1}$

Herein, the Jacobians for state and measurement can be defined as follows:

$$F_t = \left.\frac{\partial f}{\partial x}\right|_{\hat{x}_{t/t}} \; ; H_{t+1} = \left.\frac{\partial h}{\partial x}\right|_{\hat{x}_{t+1/t}} \tag{3}$$

Therefore, the process of the EKF algorithm can be presented as follows [34]:
Prediction step:

$$\hat{x}_{t+1|t} = f\left(\hat{x}_{t|t}\right); \; and \quad P_{t+1|t} = F_t P_{t/t} F_t^T + Q_t \tag{4}$$

Filtering step:

$$\hat{x}_{t+1/t+1} = \hat{x}_{t+1/t} + K_{t+1}\left[y_{t+1} - h\left(\hat{x}_{t+1/t}\right)\right] \tag{5}$$

$$K_{t+1} = P_{t+1/t} H_{t+1}^{\mathrm{T}} \left[H_{t+1} P_{t+1/t} H_{t+1}^{\mathrm{T}} + R_{t+1}\right]^{-1} \tag{6}$$

$$P_{t+1/t+1} = \left[I - K_{t+1} H_{t+1}\right] P_{t+1/t} \tag{7}$$

where K is a Kalman gain vector.

2.3. Wavelet PCA Method

The wavelet and principal component analyses (PCA) are among the most popular methods for extracting actual information from time series measurements [17,35]. The wavelet PCA (WPCA) is one of the common methods for smoothing real-time measurements [17]. This method is proposed in [17,36], and the GPS time series measurement smoothing process based on the WPCA is described below.

The methodology used to eliminate the GPS error and measurement noise is shown in Figure 1. It consists of two stages: training and reconstruction. In the training stage, the level of wavelet transformed (DWT) (*J*) of each direction of the GPS observation matrix (X) with Symlets mother wavelet is calculated using Matlab. The main steps for wavelet smoothing are decomposition of the signals into details and approximate coefficients, then thresholding elimination of small detail coefficients and signal reconstruction [36]. Herein, it is noted that the wavelet coefficients are not strongly correlated but do depend on each other [30]. Therefore, all coefficients are used in the reconstruction stage. The eigenvalues and eigenvectors are calculated from the auto-correlation matrix, and then the eigenvalues are arranged in descending order to select the eigenvectors with eigenvalues greater than 0.05 times the sum of all eigenvalues of the signals. Finally, this stage displays the original and reconstructed signals. In the reconstruction stage, the quality of the reconstructed signals (built from the training stage) is checked by calculating the relative mean square errors (should be close to 100%). From the previous stage, the numbers of retained principal components are presented. These results can improve the signals by removing noise based on killing the wavelet details at selected levels. This model returns a simplified version of the input GPS observation signals obtained from the wavelet-based PCA [30,36,37].
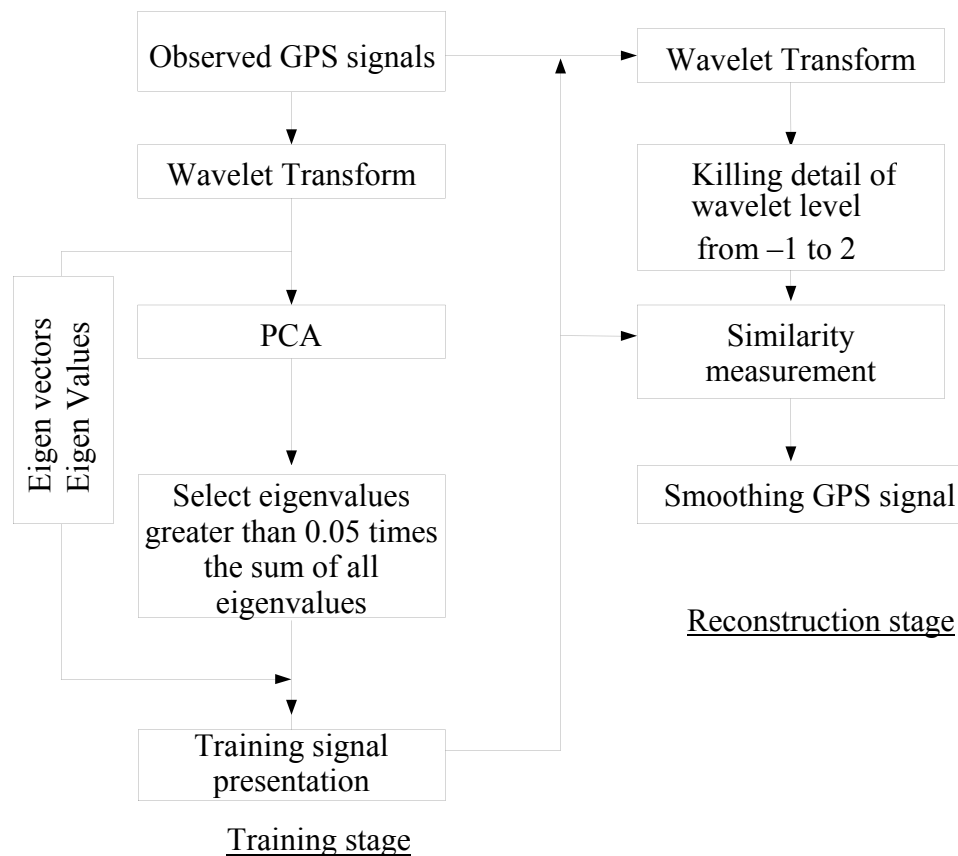
Figure 1. Block diagram of the proposed WPCA system.

On other hand, to extract the fundamental frequency of the structures from the GPS data, the Fast Fourier Transform (FFT) and short-time Fourier transform (STFT) can be applied. The two methods are presented in [30].

3. Results and Discussion

3.1. Evaluation of Method Performance

To evaluate the performance of the three methods, a real time kinematic (RTK) dual GPS monitoring system is used. The monitoring system includes a Trimble-5700 GPS receiver base and rover (the distance between the rover and the base of the GPS receivers is 10.0 m) to reduce the multipath errors. The accuracy of the GPS instruments used (Trimble 5700 GPS receiver) is 1 cm + 1 ppm (length of base line) in the horizontal direction and 2 cm + 1 ppm (length of base line) for the vertical direction, and the sampling frequency rate is 1 Hz. The rover GPS is supported on a rotating arm (1.0 m length) moved on an arc track as shown in Figure 2a, and the data collected are converted to the World Geodetic Coordinate System 1984 (WGS84). The relative coordinates (measured coordinates–mean of coordinates (DX & DY)) are collected, and the de-noised GPS signals based on the summarized methods are presented in Figures 2b and 3. The evaluation parameters utilized to evaluate the three methods are the root mean square (RMS), error positive peak (EPP), error negative peak (ENP), and signal-to-noise ratio (SNR). Table 3 presents the errors of the three methods.
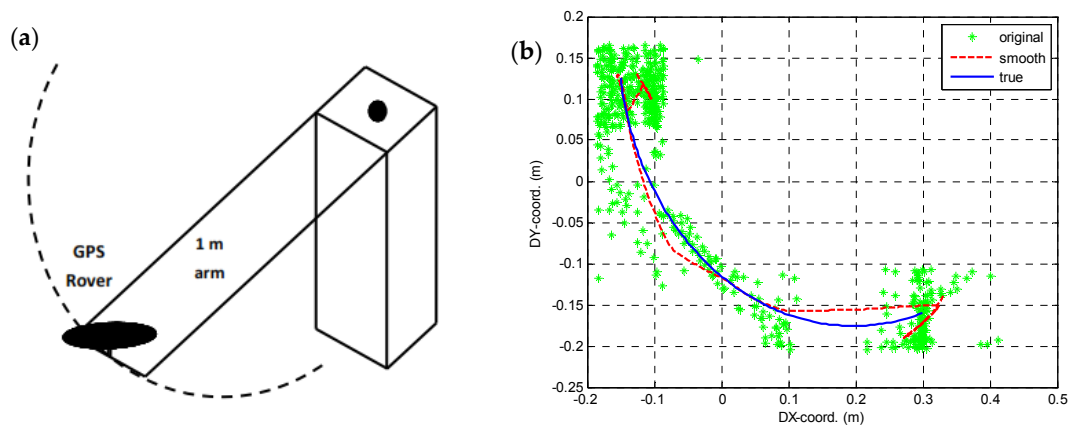
Figure 2. Experimental setup and observation: (**a**) monitoring system; (**b**) scatter measurements and adjustment.

In the RLS method, the mathematical positions of GPS are used to detect the desired (true) signals; herein, the desired signals are calculated based on the movement of the experimental arm, as shown in Figure 2b. The RLS forgetting factor is assumed to be 1, and the input signal covariance inverse matrix is $1 \times I$ (20) (I is the identity matrix). Figure 3a shows that the delay observation affects the filtered signals. The correlations between the original and filtered observations are 0.99 and 0.96 for the X and Y directions, respectively. This result means that most of the arm movement information is represented well by this method. Table 3 shows that RLS increases the accuracy of the GPS time history observations by 72% and 79% in the Y and X directions, respectively. Additionally, some information from the time history observations is lost at the beginning of the prediction position for the GPS points.
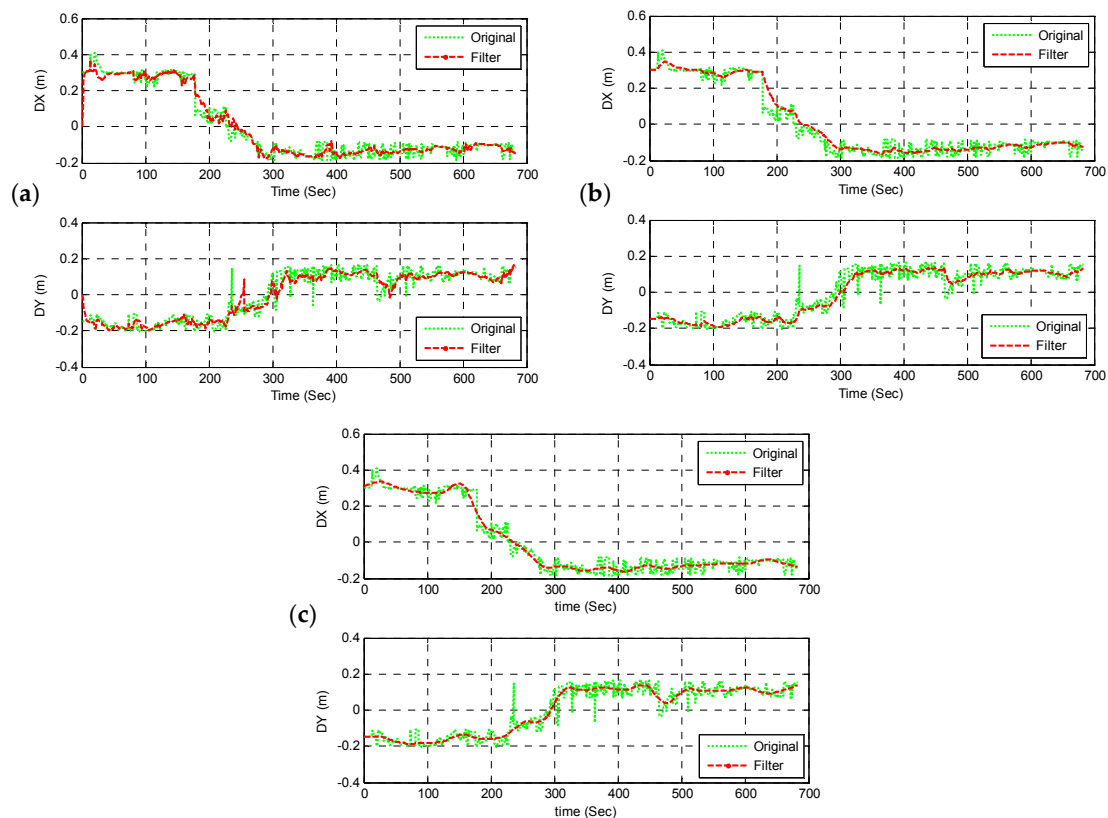

Figure 3. Evaluation of the methods used: (**a**) RLS; (**b**) KF; and (**c**) PCA.

In the EKF, a linear function is assumed between the pre and posterior state vectors because of the limited data observation. Additionally, the relationship between the observed and the state vectors is assumed to be linear to estimate the first predictive vector of the time series. Then, the nonlinear dynamic system of the GPS coordinate measurements is linearized using complex step differentiation (Jacobian), as shown in Table 2. In this section, the time delay of the filter results is not observed because the linear function is assumed in the first stage, as shown in Figure 3b. In addition, the correlations between the original and filtered observations are calculated to be 0.98 and 0.97 for the X and Y directions, respectively, which means that the EKF can represent the arm movement better than RLS. The EKF increases the accuracy of the GPS time history observation by 75% and 80% in the Y and X directions, respectively (Table 3), with no information losses from the time history of the GPS observations.

Table 3. Comparison of GPS observation time history.

Method	Direction	RMS (m)	EPP (m)	ENP (m)	SNR (dp)
RLS	X	0.035	0.125	−0.304	32.40
	Y	0.036	0.190	−0.213	25.91
EKF	X	0.034	0.0875	−0.208	33.81
	Y	0.034	0.244	−0.166	26.93
WPCA	X	0.029	0.104	−0.123	37.14
	Y	0.033	0.256	−0.184	27.59

For the WPCA method, the DWT at level 3 of each spectrum of the observation matrix X with wavelet Symlet 12 is used, and the steps of WPCA (presented in Figure 1) are applied. The results of this method show that the correlations calculated between the original and filtered observations are 0.99 and 0.98 for the X and Y directions, respectively (Figure 3c). This result means that WPCA is better than RLS and EKF in the prediction of the accurate position of the arm point movements. WPCA increases the accuracy of the GPS time history observations by 76% and 85% for the Y and X directions, respectively (Table 3), with no information loss from the GPS time history observations. Therefore, comparing the three methods, it is concluded that WPCA is the best method to detect the semi-static response of structures without information loss. Meanwhile, the statistical parameter values of the SNR and RMS show high and low values, respectively. Figure 2b shows the smoothed true and observation signals based on WPCA. The smoothed and true signals are very close. Based on these results, WPCA can be used to evaluate the static and dynamic behavior of short- and long-span bridges with low and high sampling GPS measurements. As presented in Table 3, the distortion of each direction ($d = \sqrt{\Delta x^2 + \Delta y^2}$, where Δx and Δy are the distortion of the maximum error in the X direction and Y direction, respectively) of the filtered signals with RLS, EKF, and WPCA are 0.35, 0.27, and 0.19 m, respectively. This result means that the variance in the input and output vectors for the RLS and EKF methods affects the output of the two methods. However, the variance ratio and the tracking time should be studied to improve the quality of the two methods, which is still under investigation by the authors.

3.2. Bridge Behavior Evaluation

To study the effectiveness of the low and high sampling frequency, the performance of the one and 20 Hz sampling frequencies is studied. Two case studies are presented: Mansoura Railway Bridge and the long-span Yonghe Bridge. Monitoring of the stiff point for Mansoura Bridge is discussed to assess the 1 Hz GPS errors and study the dynamic performance of the bridge. The movement evaluation of the tower of the long-span (Yonghe) bridge is studied using the 20-Hz sampling frequency, and the GPS error for this instrument is discussed.

3.2.1. Mansoura Railway Bridge Evaluation

The Mansoura railway bridge is one of the oldest bridges in Mansoura City, Egypt, connecting Mansoura and Talkha cities. Figure 4 shows the bridge and the monitoring system used. The bridge consists of four main arch truss girders, and the length of each girder is 70.0 m. This bridge is used for two types of traffic: trains in the middle (double-track) and one vehicle lane on each side of the bridge. To evaluate the response of the bridge under current train loads, a one-Hz RTK-GPS is used. The RTK survey base station is set up over stable ground, as shown in Figure 4, and the radio transmitter is attached to the monitoring system. The distance between the base station and rover positions is 188.0 m, and therefore, the accuracy of the measurements is one centimeter [38]. The RTK-GPS is used to collect raw data at a rate of 1 Hz. The measuring conditions were favorable: the receiver was free of any obstruction for a 15° angle view of the horizon, and at least four GPS satellites were tracked continuously. Trimble-5700 dual-frequency GPS receivers recording at a rate of 1 Hz were used. The data collected were post-processed using the GPS-Trimble Business Center software. The outputs of the GPS software were the time series of instantaneous Cartesian coordinates of the rover receiver in the WGS84 coordinate system (x, y, z). A local bridge coordinate system (BCS) (X, Y, Z) was established for the analysis and evaluation of the observed data. The coordinates in WGS84 are transformed into BCS coordinates by a 2D similarity transformation [17], and the movement accuracy is calculated using least squares. Herein, the X data, Y data, and Z data represent the displacement changes along the longitudinal direction, transverse direction, and altitude directions of the bridge, respectively. The receiver coordinates in the three dimensions were transformed into a time series of apparent displacements around a relative 0, representing the equilibrium level of the monitoring point, as shown in Figure 5. During the monitoring period, two trains passed across the bridge towards Mansoura.

Figure 4. Mansoura Bridge and monitoring system: (**a**) bridge view; (**b**) base station GPS; (**c**) rover GPS.

The stiff point movement is monitored (Figure 4c) to assess the dynamic extraction for the 1 Hz GPS monitoring system, as well as to evaluate the accuracy of the WPCA estimation. Figure 5 illustrates the time series monitoring system and the WPCA smoothed movement with and without trains passing during the monitoring time. The extracted smoothed movements show that the 1-Hz GPS can be used to estimate the semi-static movement components, whereas the maximum deformation occurred when

a train passed across the bridge. In addition, the maximum variation in the X, Y, and Z directions with train number one are 40.12, 30.68, and 134.89 mm, respectively, and with train number two are 47.06, 25.08, and 118.14 mm, respectively. Moreover, the maximum variation between the two trains is 24.77, 15.13, and 50.08 mm for the X, Y, and Z directions, respectively. The statistical parameter analyses (maximum (Max), minimum (Min), mean (M), and standard deviation (SD)) for the three directions and for the original and smoothed signals are summarized in Table 4.
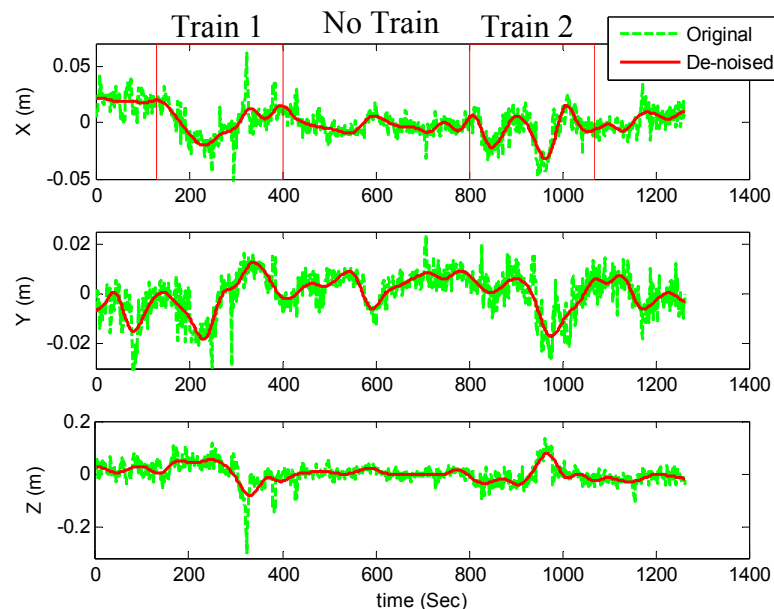

Figure 5. Measured and smoothed relative time series movements of the bridge.

Figure 5 and Table 4 show that the accuracy of the smoothed movements of the measurements are increased by 25%, 21%, and 27% for the X, Y, and Z directions, respectively, in the case of Train 1 and by 29%, 25%, and 45% for the X, Y, and Z directions, respectively, when no trains are crossing the bridge. Therefore, it can be concluded that WPCA is suitable for detecting the actual behavior of the bridge in the time domain. The accuracy of the measurements is affected (decreased) when the bridge is loaded (train passing) because the dynamic noise and error contaminated the GPS measurements [5,8].

Table 4. Statistical parameters of the bridge movements.

Event	Parameters	Original			Smoothed		
		X (mm)	Y (mm)	Z (mm)	X (mm)	Y (mm)	Z (mm)
Train No.1	Max	61.82	16.38	118.39	19.59	12.46	52.67
	Min	−53.69	−29.96	−298.60	−20.53	−18.22	−82.22
	M	-3.52×10^{-2}	−1.10	5.81	-1.93×10^{-1}	−1.13	6.18
	SD	±16.38	±9.96	±59.41	±12.18	±8.70	±42.76
No Train	Max	29.67	23.50	59.39	15.06	9.12	20.86
	Min	−32.30	−12.57	−107.60	−9.71	−6.01	−29.22
	M	−2.27	3.73	2.27	−2.17	3.80	1.83
	SD	±7.55	±5.44	±17.51	±5.35	±4.07	±9.42
Train No.2	Max	23.91	19.77	132.59	14.96	7.77	76.82
	Min	−47.01	−25.90	−94.60	−32.10	−17.31	−41.32
	M	−6.73	−1.78	−5.69	−6.82	−1.81	−5.30
	SD	±15.32	±9.56	±41.84	±12.46	±7.40	±33.19

Moreover, the time series evaluation of the bridge movements shows that the maximum movements occurred in the Z direction in both load cases. In addition, the maximum movement

in the X direction when the bridge was empty (no train passes) was higher than in the Y direction, which means that the errors in the X direction are significant. The mean movements of the bridge are small and insignificant in both load cases, which means that the bridge movement is safe under the effect of train loads. Additionally, it is noted that a long-period monitoring system should be designed and installed on the bridge to evaluate the full behavior of the bridge under train loads and environmental effects.

From Table 4, the highest movements of the bridge are observed in the Z direction. Therefore, the frequency domain of the Z direction is considered to study the dynamic behavior of the bridge. The FFT is used to extract the frequency component of the three loading cases for the bridge. The frequency and power spectrum density are calculated. A threshold of three times the SD of the calculated short period is applied to remove the errors in the GPS positions and maintain the normality of the probability distribution of the measurements. In addition, a finite impulse response filter (designed by Matlab is used to eliminate the dynamic noises. The short-period bridge movement and frequency components of the loading cases are presented in Figure 6. The rigid monitoring point selected is used to extract the dynamic noise of the GPS measurements, as shown in Figure 6. The PSD measurements components of the unloading case show smaller values than the loaded cases, and the dominant frequency is 0.093 Hz.
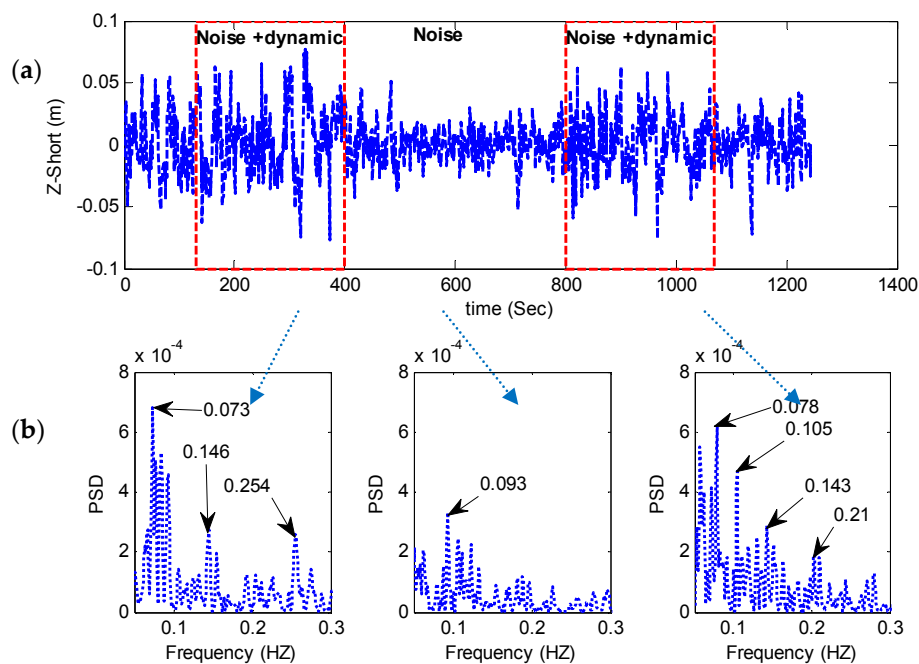

Figure 6. The short-period component and frequency components of the bridge movements: (**a**) short-period; (**b**) frequency components of the bridge loading cases.

The amplitude of the short-period movement component is higher than in the unloading case. The frequency components are presented in Figure 6b. The frequency modes of the first train case are 0.073, 0.146, and 0.254 Hz, while in the second train case they are 0.078, 0.105, 0.143, and 0.21 Hz. The frequency component of the GPS measurements shows that the noise can be affected up to 0.093 Hz, in this case. However, the first three frequency mode components of the bridge are 0.105, 0.146, and 0.21 Hz. From the results of the time series and frequency components, it is concluded that the noise in the GPS used is high, and the data smoothed using the FFT can be used to extract the movements and frequency modes of the components. Furthermore, the frequency components are limited in this case, as the structure frequency modes of more than 0.3 Hz cannot be estimated [23].

3.2.2. Yonghe Long-Span Bridge Evaluation

The Yonghe Bridge is one of the oldest long-span bridges in mainland China. Figure 7 depicts the bridge and the GPS monitoring system. The structure of the bridge is a cable-stayed pre-stressed concrete with double pylons, with a main span of 260.0 m. The entire width of the bridge deck is 13.6 m, including road lanes of 9.0 m and sidewalks on both sides of the bridge. More details on the bridge construction materials and properties can be found in [39]. In 2007, a long-term SHM system was designed and has been used as presented in [9,38,40]. Two GPS rover receivers are installed at the top of the two towers (north, N and south, S), and one base station is clamped at a bank near the bridge (Figure 7b). The receivers used are LEICA-GMX902 antenna with sampling of 20 Hz. The output of the two rovers is the RTK time series of global Cartesian coordinates of the installed receivers in the WGS84 coordinate system. Therefore, the collected coordinate data are converted to a local BCS for the analysis of the observations [41]. In this coordinate system, the X-axis represents the traffic direction, and the Y-axis represents the lateral direction of the bridge (Figure 7b). The analysis of the movements is focused on the plane (X, Y) coordinates. This coordinate system allows evaluation of the performance of the structure and describes its movement in relation to the movement directions of the structure. During the bridge inspection on August 2008, several damage patterns were detected near the south tower [39]. The dynamic performance of the bridge is studied based on a long-period monitoring system; see [39,41,42]. Moreover, the quality of the GPS observations is discussed in [41]. However, in this section, the filtering model is evaluated in damaged and undamaged cases, and the dynamic performance of the two cases is presented and discussed for the GPS installed on the south tower.
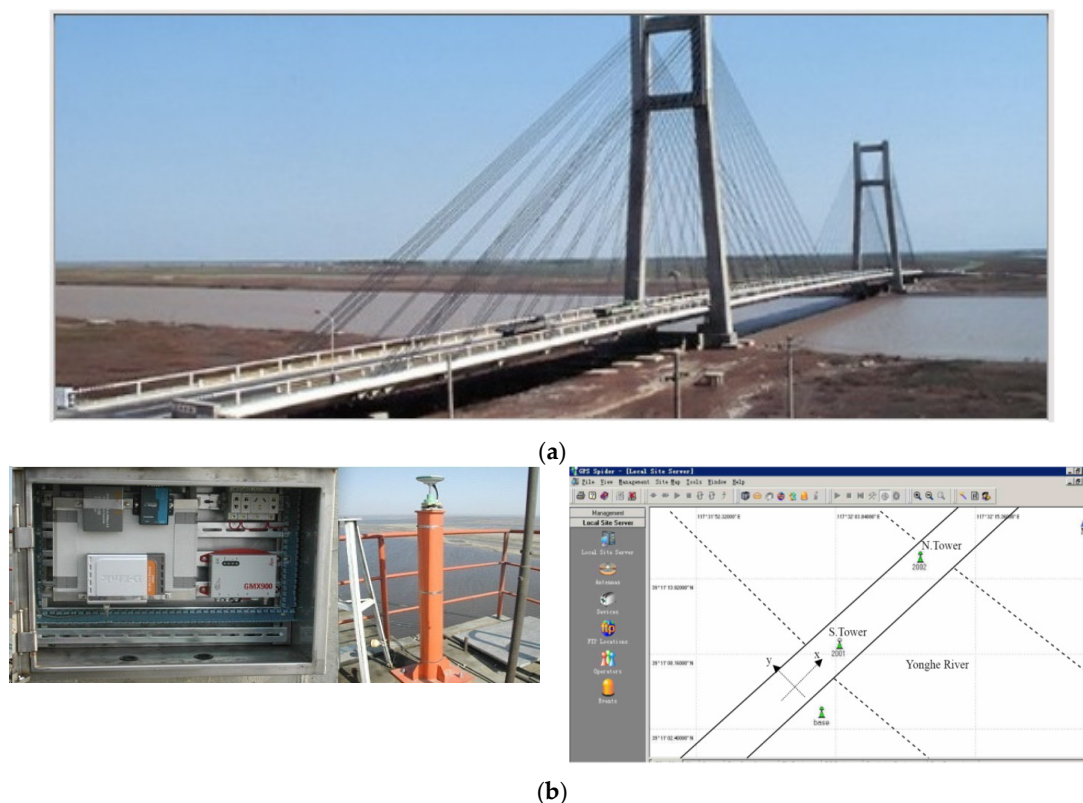

(**a**)

(**b**)

Figure 7. Yonghe Bridge: (**a**) view and (**b**) GPS monitoring system.

Two days are selected to evaluate the filtering method and bridge performance during healthy and damaged cases, namely, 30 December 2007 (Healthy, H) and 16 June 2008 (Damaged, D). The H case is selected after the opening of the bridge following its maintenance on September 2007. The D

case is selected based on a previous study [42]; bridge damage occurred before this date. The GPS measurements and the WPCA-smoothed signals of the two cases are shown in Figure 8. To detect the effect of the de-noising methods, the Y direction measurements in the H case are used to evaluate the noises in this direction. This direction is selected because the rigidity of the tower in the Y direction is high. The standard deviations of the Y direction for the observed and smoothed signals are 2.73 and 2.52 mm, respectively. This result means that the WPCA method improves the high sampling frequency of the GPS measurements and can be used to eliminate measurement errors. In addition, the correlation coefficient between the observed and smoothed signals is 0.92. However, it is noted that the accuracy of the measurements increased without loss of information on the bridge movements. In addition, the bridge's semi-static behavior can be detected in both directions in both cases, as shown in Figure 8. Therefore, it is concluded that the WPCA method can be utilized to detect the actual bridge behavior without information loss regarding the bridge movements.

The H case observations show that the X direction movements are noisy. The maximum de-noised movements in the X and Y directions are 24.75 and 8.15 mm, respectively. Furthermore, the correlation coefficient between the movements of the two directions is -0.01. This result means that the effective movements of the tower occurred in the traffic direction (X-direction), as discussed in [41], and this conclusion confirms that the noise also occurred in this direction. Other previous studies [9,41,42] concluded that the traffic loads are the main loads affecting the bridge. The GPS measurements clearly show that the peak impulses are caused by traffic loads. Furthermore, each measurement peak point corresponds to the time when traffic crosses the bridge. However, it is noted that the smoothed signals refer to the semi-static movements of the bridge tower, and the remaining signals refer to the dynamic performance, which includes the traffic load effects and GPS errors. Additionally, no correlation is observed between the two directions. As such, the tower is not affected in the Y direction due to its rigidity.

The D case measurements show that the X and Y directions movements are both noisy. The maximum de-noised movements of the X and Y directions are 249.61 and 18.18 mm, respectively. The correlation coefficient between the movements in the two directions is 0.45. This result means that the free movements of the tower in the two directions can be concluded in this case. In addition, the maximum movement of the two directions is observed at the same time (2.2 h), as shown in Figure 8b; in addition, some misreadings are observed at that time. Therefore, the WPCA method tried to estimate the misreading data based on previous observations. The noisy observations occurred due to damage, traffic load and GPS errors. Accordingly, on 31 July 2008, loads on the bridge were limited to avoid its collapse [39]. On the other hand, it is observed that the semi-static movements in the H case are higher than in the D case. This result means that the damage affects the behavior of the bridge in both the static and dynamic cases.
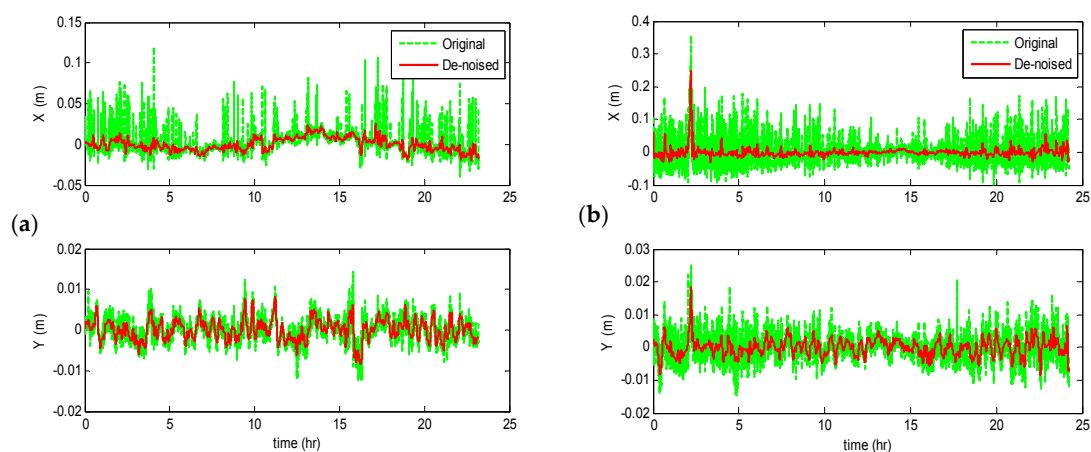

Figure 8. Measured and smoothed GPS observations for the (**a**) healthy; and (**b**) damaged cases.

The X direction is selected to evaluate the behavior of the bridge in the two cases H and D. Figure 9 illustrates the short-period components of the two cases. In addition, the frequency components are presented using FFT and STFT. Table 5 presents the time series statistical analysis parameters (the absolute maximum (Max) and mean (M) values and the SD) for the short-period movements in both cases. From Figure 9a and Table 5, the impulse from traffic effects is shown clearly in the H case. The movements of the tower in the healthy case are more stable than in the damaged case, while the maximum movement ranges are 21.17 and 191.03 mm for the H and D cases, respectively. Moreover, the accuracy of the short-period measurements of the damaged case decreased by 70% relative to the healthy case. In addition, the absolute mean and maximum measurements of the damaged case are higher than in the healthy case.
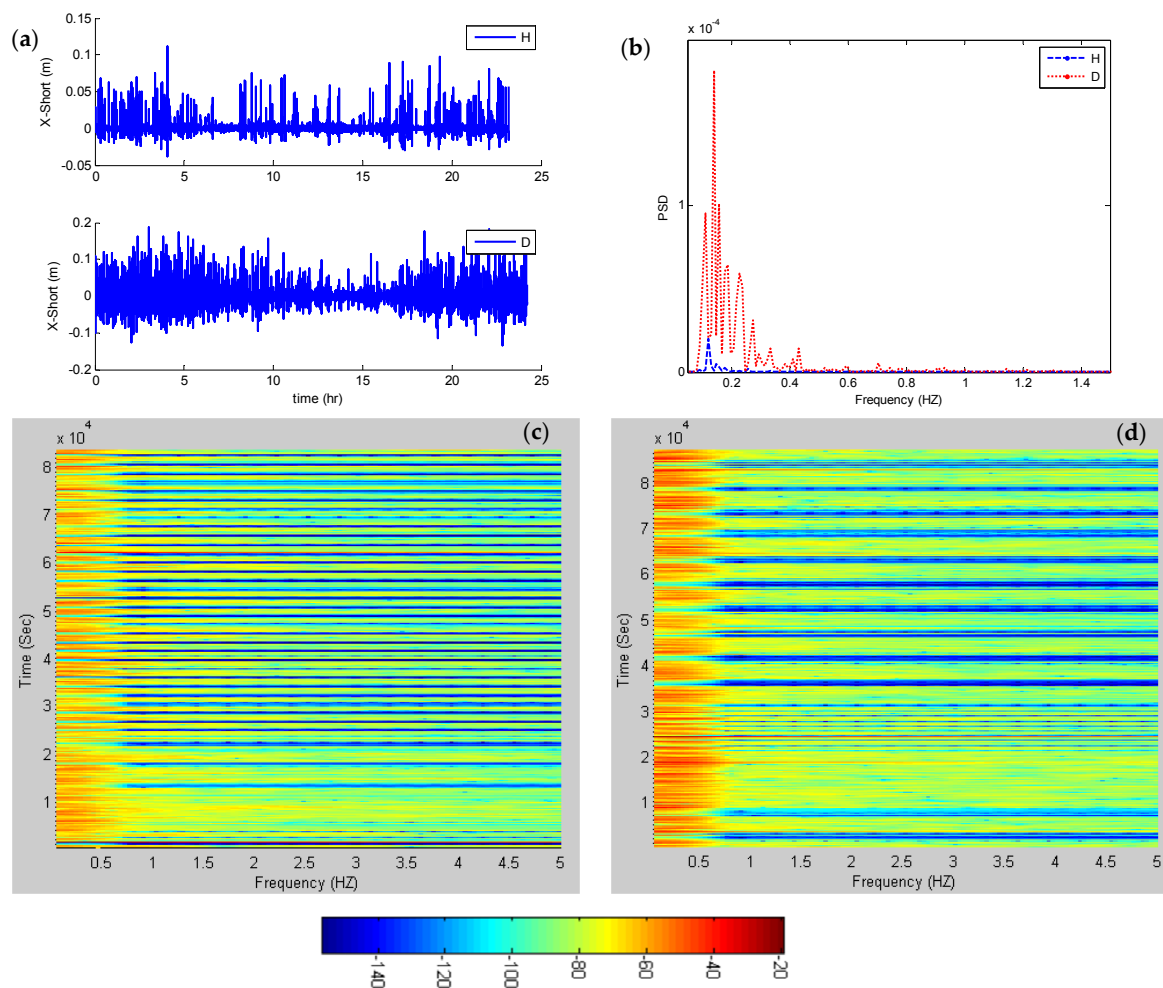

Figure 9. The dynamic analysis of the short-period components of the H and D cases: (**a**) time series; (**b**) FFT components; (**c**) STFT of H; (**d**) STFT of D.

The frequency components of the two cases are presented in Figure 9b–d. The dominant frequencies are 0.14 and 0.12 Hz for the D and H cases, respectively. Additionally, the frequency modes can be observed and detected up to 1 Hz. The PSD values for the dominant frequency are 1.82×10^{-4} and 2.08×10^{-5} dB for the two cases, respectively. In addition, the PSD values are high during the monitoring day in the damaged case, as shown in Figure 9c,d, with a high jump in the frequency component. Therefore, the healthy state is more stable in both the time and frequency components.

Table 5. Statistical parameters of the short-period movements for the healthy and damaged cases.

Parameters	H	D
Max (mm)	112.23	186.78
M (mm)	3.67	16.00
SD (mm)	±7.77	±25.70

4. Summary and Conclusions

In this study, nonlinear filtering and smoothing methodologies are applied to estimate a suitable method for detecting the movement components of structures with low- and high-frequency GPS sampling rates. The nonlinear RLS, EKF, and WPCA methods are selected to compare the effectiveness of filtering and smoothing techniques. Two case studies are presented and evaluated. First, the Mansoura railway bridge is selected to evaluate the loading and unloading cases of the bridge with 1 Hz GPS sampling frequency. Second, the Yonghe Bridge is selected to evaluate the healthy and damaged cases of the bridge using 20 Hz GPS sampling frequency. Based on the results of the evaluation methods, the following conclusions are reached:

The WPCA method shows better results and can be used to detect the semi-static response of structures without information loss regarding the structure behavior. Moreover, frequency domain analysis of the bridges shows that the bridges' dynamic performance can be extracted after GPS measurement adjustment. Therefore, the WPCA can be used to evaluate the static and dynamic behavior of short- and long-span bridges with low and high sampling frequency GPS measurements.

The WPCA is suitable for detecting the actual behavior of Mansoura Bridge in the time domain. Moreover, the loading case is affected by the accuracy of the measurements because the dynamic noise and error contaminated the GPS measurements. The extracted smoothed movements of the bridge show that the 1 Hz GPS can be used to estimate the semi-static movement components. Evaluation of the time series of the bridge movements shows that the maximum movements occurred in the Z direction in both loading cases, with small and insignificant movements of the bridge in both cases. This result means that the bridge movement is safe under train loads. Furthermore, the first three frequency mode components of the bridge based on a 1 Hz GPS monitoring system are 0.105, 0.146, and 0.21 Hz. In addition, the frequency components showed that the noise of the GPS used is high, and the data smoothed using the FFT can be used to extract the movement components and frequency modes.

The measurements of the 20 Hz GPS monitoring system show high noise in both monitoring cases of Yonghe Bridge. The noisy observations of the system were due to damage, traffic load, and GPS error. The correlation coefficient between the plane movements of the bridge is small in the healthy case. In addition, the movements of the X and Y directions increased by 90% and 55%, respectively. Furthermore, the damage affects the behavior of the bridge in the static and dynamic cases. The frequency components of the two cases show that the dominant frequencies are 0.14 and 0.12 Hz for the damaged and healthy cases, respectively. Moreover, the frequency modes can be observed and detected up to 1 Hz. Furthermore, the PSD for the dominant frequency is higher during the monitoring day in the damaged case.

Finally, it can be concluded that the WPCA method is effective with both low and high sampling frequencies of GPS monitoring systems. Additionally, the low and high sampling frequency GPS techniques are suitable for extracting the movement components of structures in the time domain, while the high sampling frequency GPS instruments are suitable for detecting the dynamic behavior of structures.

Author Contributions: Mosbeh R. Kaloop conceived the study, performed the analysis, wrote the paper, and interpreted the results. Mosbeh R. Kaloop, Jong Wan Hu and Emad Elbeltagi collected the data, reviewed the study plan, and edited the manuscript.

Conflicts of Interest: The authors declare no conflict of interest.

References

1. Im, S.B.; Hurlebaus, S.; Kang, Y.J. Summary review of GPS technology for structural health monitoring. *J. Struct. Eng.* **2013**, *139*, 1653–1664. [CrossRef]
2. Yi, T.H.; Li, H.N.; Gu, M. Recent research and applications of GPS-based monitoring technology for high-rise structures. *Struct. Control Health Monit.* **2013**, *20*, 649–670. [CrossRef]
3. Moschas, F.; Stiros, S. Noise characteristics of high-frequency, short-duration GPS records from analysis of identical, collocated instruments. *Meas. J. Int. Meas. Confed.* **2013**, *46*, 1488–1506. [CrossRef]
4. Amiri-Simkooei, A.R.; Tiberius, C.; Teunissen, P.J.G. Noise characteristics in high precision GPS positioning. In Proceedings of the 6th Hotine-Marussi Symposium on Theoretical and Computational Geodesy, Wuhan, China, 29 May–2 June 2006.
5. Nickitopoulou, A.; Protopsalti, K.; Stiros, S. Monitoring dynamic and quasi-static deformations of large flexible engineering structures with GPS: Accuracy, limitations and promises. *Eng. Struct.* **2006**, *28*, 1471–1482. [CrossRef]
6. Moschas, F.; Stiros, S. Measurement of the dynamic displacements and of the modal frequencies of a short-span pedestrian bridge using GPS and an accelerometer. *Eng. Struct.* **2011**, *33*, 10–17. [CrossRef]
7. Yu, J.; Meng, X.; Shao, X.; Yan, B.; Yang, L. Identification of dynamic displacements and modal frequencies of a medium-span suspension bridge using multimode GNSS processing. *Eng. Struct.* **2014**, *81*, 432–443. [CrossRef]
8. Moschas, F.; Stiros, S. Dynamic deflections of a stiff footbridge using 100-Hz GNSS and accelerometer data. *J. Surv. Eng.* **2015**. [CrossRef]
9. Kaloop, M.R.; Li, H. Multi input-single output models identification of tower bridge movements using GPS monitoring system. *Meas. J. Int. Meas. Confed.* **2014**, *47*, 531–539. [CrossRef]
10. Yi, T.H.; Li, H.N.; Gu, M. Experimental assessment of high-rate GPS receivers for deformation monitoring of bridge. *Meas. J. Int. Meas. Confed.* **2013**, *46*, 420–432. [CrossRef]
11. Kaloop, M.R.; Hu, J.W. Optimizing the de-noise neural network model for GPS time-series monitoring of structures. *Sensors* **2015**, *15*, 24428–24444. [CrossRef] [PubMed]
12. Feng, M.Q.; Fukuda, Y.; Chen, Y.; Soyoz, S.; Lee, S. *Long-Term Structural Performance Monitoring of Bridges. Phase II: Development of Baseline Model and Methodology—Report to the California Department of Transportation*; CA07-0245; Department of Civil and Environmental Engineering University of California: Irvine, CA, USA, 2008.
13. Gomez-Gil, J.; Ruiz-Gonzalez, R.; Alonso-Garcia, S.; Gomez-Gil, F.J. A Kalman filter implementation for precision improvement in Low-Cost GPS positioning of tractors. *Sensors* **2013**, *13*, 15307–15323. [CrossRef] [PubMed]
14. Chen, X.; Gao, Z. Data processing based on wavelet analysis in structure health monitoring system. *J. Comput.* **2011**, *6*, 2686–2691. [CrossRef]
15. Ding, Y.; Li, A.Q. Structural health monitoring of long-span suspension bridges using wavelet packet analysis. *Earthq. Eng. Eng. Vib.* **2007**, *6*, 289–294. [CrossRef]
16. Ogundipe, O.; Lee, J.K.; Roberts, G.W. Wavelet de-noising of GNSS based bridge health monitoring data. *J. Appl. Geod.* **2014**, *8*, 273–281. [CrossRef]
17. Kaloop, M.R.; Kim, D. De-noising of GPS structural monitoring observation error using wavelet analysis. *Geomat. Nat. Hazards Risk* **2016**, *7*, 804–825. [CrossRef]
18. Oussalah, M.; De Schutter, J. Adaptive Kalman filter for noise identification. *Int. Conf. Noise Vib. Eng.* **2000**, *3*, 1–8.
19. Bhatt, D.; Aggarwal, P.; Devabhaktuni, V.; Bhattacharya, P. A novel hybrid fusion algorithm to bridge the period of GPS outages using low-cost INS. *Expert Syst. Appl.* **2014**, *41*, 2166–2173. [CrossRef]
20. Hwang, J.; Yun, H.; Park, S.K.; Lee, D.; Hong, S. Optimal methods of RTK-GPS/accelerometer integration to monitor the displacement of structures. *Sensors* **2012**, *12*, 1014–1034. [CrossRef] [PubMed]
21. Chan, W.S.; Xu, Y.L.; Ding, X.L.; Dai, W.J. An integrated GPS-accelerometer data processing technique for structural deformation monitoring. *J. Geod.* **2006**, *80*, 705–719. [CrossRef]

22. Meng, X.; Wang, J.; Han, H. Optimal GPS/accelerometer integration algorithm for monitoring the vertical structural dynamics. *J. Appl. Geod.* **2014**, *8*, 265–272. [CrossRef]

23. Elnabwy, M.T.; Kaloop, M.R.; Elbeltagi, E. Talkha steel highway bridge monitoring and movement identification using RTK-GPS technique. *Meas. J. Int. Meas. Confed.* **2013**, *46*, 4282–4292. [CrossRef]

24. Sharma, O.; Janyani, V.; Sancheti, S. Recursive least squares adaptive filter a better ISI compensator. *Int. J. Electron. Circuits Syst.* **2009**, *3*, 40–45.

25. Chen, Y.; Le-Ngoc, T.; Champagne, B.; Xu, C. Recursive least squares constant modulus algorithm for blind adaptive array. *IEEE Trans. Signal Process.* **2004**, *52*, 1452–1456. [CrossRef]

26. Budura, G. Nonlinear systems identification using the Volterra model. *Int. Symp. Syst. Theory* **2005**, *1*, 25–30.

27. Mathews, V.J. Adaptive polynomial filters. *IEEE Signal Process. Mag.* **1991**, *8*, 10–26. [CrossRef]

28. Volterra Series and Nonlinear Adaptive Filters. Available online: http://guillaume.perrin74.free.fr/ChalmersMT2012/Papers/NonLinearFiltering/seminar04.pdf (accessed on 20 August 2016).

29. Haykin, S. *Adaptive Filter Theory Fifth Edition*; Pearson: Upper Saddle River, NJ, USA, 2014.

30. Trauth, M.H. *Matlab®Recipes for Earth Sciences: Second Edition*; Springer: Berlin, Germany, 2007.

31. Cuevas, E.; Zaldivar, D.; Rojas, R. Kalman filter for vision tracking. *Measurement* **2005**, *8*, 1–18.

32. Yang, J.N.; Pan, S.; Huang, H. An adaptive extended Kalman filter for structural damage identifications II: Unknown inputs. *Struct. Control Heal. Monit.* **2007**, *44*, 497–521. [CrossRef]

33. Zhang, H.; Foliente, G.C.; Yang, Y.; Ma, F. Parameter identification of inelastic structures under dynamic loads. *Earthq. Eng. Struct. Dyn.* **2002**, *31*, 1113–1130. [CrossRef]

34. Ribeiro, M.I. Kalman and extended Kalman filters: Concept, derivation and properties. *Inst. Syst. Robot. Lisboa Port.* **2004**, *2*, 1–44.

35. Fourie, S. Advanced process monitoring using wavelet and non-linear principal component analysis. Master's Thesis, Faculty of Engineering, University of Pretoria, Hatfield, South Africa, 2002.

36. Bakshi, B.R. Multiscale PCA with application to multivariate statistical process monitoring. *AIChE J.* **1998**, *44*, 1596–1610. [CrossRef]

37. Kaloop, M.; Elbeltagi, E.; Elnabwy, M. Bridge monitoring with wavelet principal component and spectrum analysis based on GPS measurements: Case study of the Mansoura Bridge in Egypt. *J. Perform. Constr. Facil.* **2015**. [CrossRef]

38. Berber, M.; Arslan, N. Network RTK: A case study in Florida. *Meas. J. Int. Meas. Confed.* **2013**, *46*, 2798–2806. [CrossRef]

39. Li, S.; Li, H.; Liu, Y.; Lan, C.; Zhou, W.; Ou, J. SMC structural health monitoring benchmark problem using monitored data from an actual cable-stayed bridge. *Struct. Control Heal. Monit.* **2014**, *21*, 156–172. [CrossRef]

40. Li, H.; Li, S.; Ou, J.; Li, H. Reliability assessment of cable-stayed bridges based on structural health monitoring techniques. *Struct. Infrastruct. Eng.* **2012**, *8*, 829–845. [CrossRef]

41. Kaloop, M.R.; Hu, J.W. Dynamic performance analysis of the towers of a Long-Span bridge based on GPS monitoring technique. *J. Sensors* **2016**. [CrossRef]

42. Kaloop, M.R.; Hu, J.W. Stayed-cable bridge damage detection and localization based on accelerometer health monitoring measurements. *Shock Vib.* **2015**. [CrossRef]